Synchrotron X-ray absorption spectroscopy of melanosomes in vertebrates and cephalopods: implications for the affinity of *Tullimonstrum*

Christopher S. Rogers[1], Timothy I. Astrop[1], Samuel M. Webb[2], Shosuke Ito[3], Kazumasa Wakamatsu[3] and Maria E. McNamara[1]

[1]School of Biological, Earth and Environmental Sciences, University College Cork, Distillery Fields, North Mall, Cork T23 TK30, Republic of Ireland
[2]Stanford Synchrotron Radiation Lightsource, SLAC National Accelerator Laboratory, 2575 Sand Hill Road, Menlo Park, CA 94025, USA
[3]Department of Chemistry, Fujita Health University School of Health Sciences, Toyoake, Aichi 470-1192, Japan

CSR, 0000-0001-7928-6280; MEM, 0000-0003-0968-4624

Screening pigments are essential for vision in animals. Vertebrates use melanins bound in melanosomes as screening pigments, whereas cephalopods are assumed to use ommochromes. Preserved eye melanosomes in the controversial fossil *Tullimonstrum* (Mazon Creek, IL, USA) are partitioned by size and/or shape into distinct layers. These layers resemble tissue-specific melanosome populations considered unique to the vertebrate eye. Here, we show that extant cephalopod eyes also show tissue-specific size- and/or shape-specific partitioning of melanosomes; these differ from vertebrate melanosomes in the relative abundance of trace metals and in the binding environment of copper. Chemical signatures of melanosomes in the eyes of *Tullimonstrum* more closely resemble those of modern cephalopods than those of vertebrates, suggesting that an invertebrate affinity for *Tullimonstrum* is plausible. Melanosome chemistry may thus provide insights into the phylogenetic affinities of enigmatic fossils where melanosome size and/or shape are equivocal.

Keywords:
fossil soft tissues, Konservat-Lagerstätten, melanosomes, trace metals

Authors for correspondence:
Christopher S. Rogers
e-mail: christopher.rogers@ucc.ie
Maria E. McNamara
e-mail: maria.mcnamara@ucc.ie

1. Introduction

Screening pigments are an essential component of visual systems in animals as they absorb errant light, thus allowing directional photoreception and the protection of photoreceptors from ultraviolet radiation [1]. Invertebrate screening pigments include ommochromes, pterines and, less frequently, melanin [2]. In contrast, the primary screening pigment in vertebrates is melanin, occurring as melanosomes (membrane-bound organelles) in the iris, choroid, retinal pigmented epithelium (RPE) [3] and sclera [4] (figure 1). RPE melanosomes include spherical and elongate forms that are partitioned spatially [5]. In bright incident light, elongate melanosomes migrate to the apical processes of RPE cells, thus protecting photosensitive pigments in photoreceptor cells from bleaching. Intriguingly, the eyes of the enigmatic taxon *Tullimonstrum gregarium* (Carboniferous, Mazon Creek, IL, USA) also exhibit successive layers of melanosomes of different geometries. This feature was interpreted as evidence of a vertebrate affinity based on a review of melanosome distribution and morphology in extant animals [2]. Whether invertebrate eye melanosomes are organized into successive tissue layers as in vertebrates is, however, unknown. Resolving this requires systematic investigation of screening pigments in invertebrate eyes. Cephalopods are an ideal test case because they, like vertebrates, possess a complex camera-style eye with multiple pigmented tissue layers [6] and are known to produce melanosomes (in the ink sac [7,8]). We systematically characterized the anatomical location and chemistry of pigmented tissues, and the geometry of pigment granules, in the eyes of the common octopus (*Octopus vulgaris*), European squid (*Loligo vulgaris*),

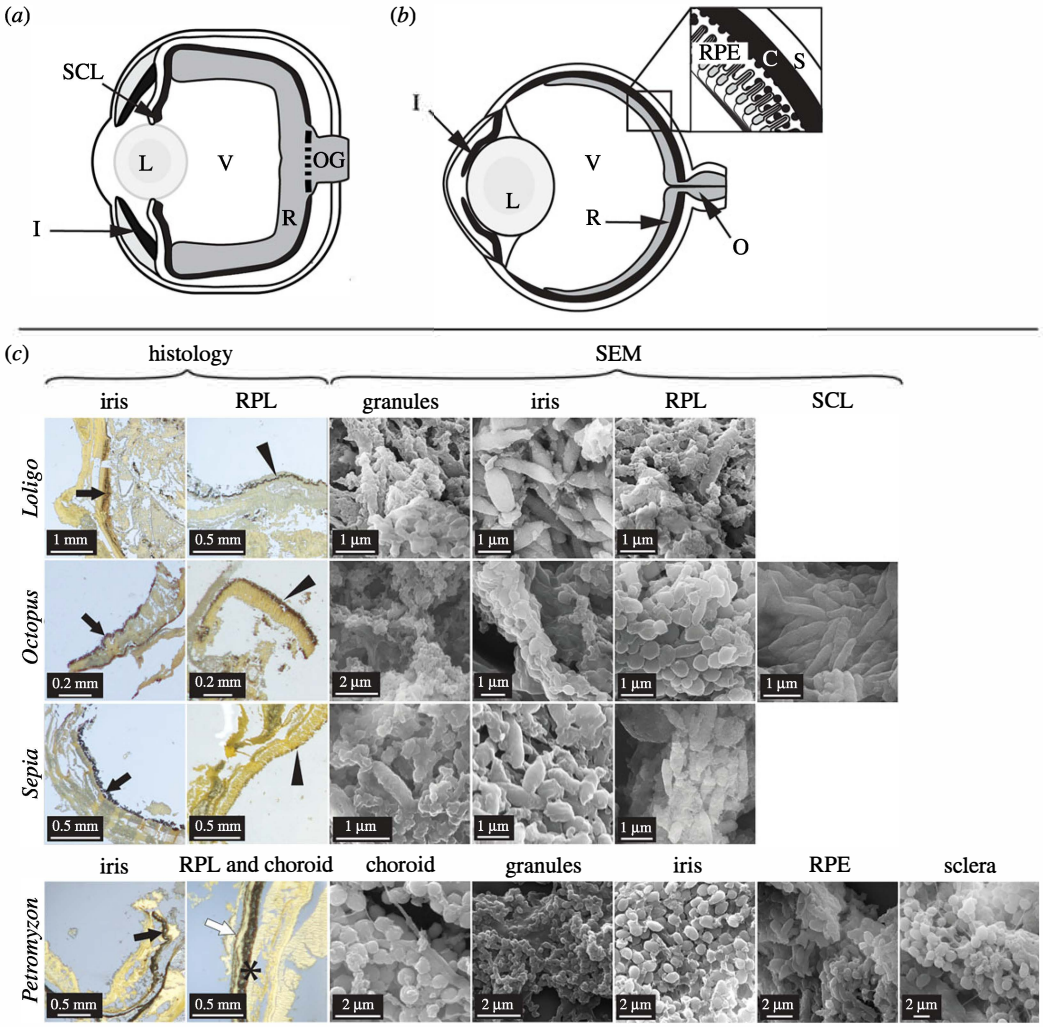

Figure 1. Anatomy of extant cephalopod and vertebrate eyes. Schematic illustrations of (*a*) cephalopod eye and (*b*) vertebrate eye with, inset, detail of tissue layers. (*c*) Histological sections and scanning electron micrographs (SEM) of eyes in *Loligo*, *Octopus*, *Sepia* and *Petromyzon*. Sections are stained with Warthin–Starry; melanin appears black. All tissues show melanosome-like microbodies. C, choroid; I/black arrows, iris; L, lens; O, optic nerve; OG, optic nerve ganglia; R, retina; RPE/*, retinal pigment epithelium; RPL/arrowheads, retinal pigmented layer; S/white arrow, sclera; SCL, subciliary layer; V, vitreous humour. (Online version in colour.)

common cuttlefish (*Sepia officianalis*), sea lamprey (*Petromyzon marinus*) and European bass (*Dicentrachus labrax*), coupled with data from fossils (electronic supplementary material, table S1). Tissues were analysed using Warthin–Starry histological staining, alkaline hydrogen peroxide oxidation (AHPO [9,10]) and scanning electron microscopy (SEM). In the eyes of extant vertebrates, melanin reduces oxidative stress by chelating metal ions [11] and recent work shows that vertebrate melanosomes have tissue-specific trace element chemistries [12]. We therefore tested whether trace element chemistry can discriminate vertebrate and cephalopod eye melanosomes using synchrotron rapid scanning-X-ray fluorescence (SRS-XRF) and X-ray absorption near edge structure (XANES) spectroscopy.

2. Material and methods

(a) Modern and fossil specimens

Specimens of *Octopus*, *Sepia*, *Loligo*, *Petromyzon* and *Dicentrachus* (each $n = 5$) were obtained from commercial suppliers (Ballycotton Seafoods and K O'Connell Fish Merchants (English Market in Cork, Republic of Ireland) and Online Baits UK). The lampreys were supplied frozen and dissected immediately after defrosting; the cephalopods and European bass were deceased at the time of purchase and were dissected within 24 h after death. Eyes were fixed in 2.5% glutaraldehyde for 1 h at room temperature, dehydrated in ethanol and stored in 70% ethanol prior to further analysis.

This study includes analysis of the eyespots of the following eight fossils: from Mazon Creek, two specimens of *Tullimonstrum* (CKGM F 6426 and FMNH PE 22061), one specimen each of the vertebrates *Mayomyzon peickoensis* (FMNH PF 5688) and *Gilpichthys greenei* (FMNH PF 8474) and the sole specimen of the fossil cephalopod *Pohlsepia mazonensis* (FMNH PE 51727); from Green River (Eocene, Colorado/Utah/Wyoming), one specimen of *Knightia* sp. (FOBU 17591) and from the Fur Formation (Eocene, Denmark) an undetermined Teterodontiformes (NHMD 199838); from the Hâkel and Hâdjoula Lagerstätte (Late Cretaceous, Lebanon), the fossil octopus *Keuppia* sp. (NHMUK PICC651A). Institutional abbreviations: NHMUK, Natural History Museum London; NHMD, Natural History Museum of Denmark; FMNH, Field Museum of Natural History; CKGM, Cork Geological Museum; FOBU, Fossil Butte National Monument.

(b) Alkaline hydroxide peroxide oxidation and hydroiodic acid hydrolysis

Tissues were dissected using sterile tools, placed in glass vials, freeze-dried and powdered. The vertebrate choroid and RPE could not be separated and thus were treated as a single tissue in this analysis. Freeze-dried tissue samples (9–17 mg) were homogenized in water with a Ten-Broeck homogenizer at a concentration of 10 mg ml^{-1} and 100 µl or 200 µl aliquots processed using AHPO [9] and hydroiodic acid hydrolysis [10]. AHPO after HCl hydrolysis tests for the presence of pyrrole-2,3,5-tricarboxylic acid (a marker for eumelanin [9]); hydroiodic acid analysis tests for the presence of 4-amino-3-hydroxylphenylalanine (a marker for phaeomelanin [10]).

(c) Histology

Dissected samples of tissues from cephalopod eyes and choroid, iris, RPE and sclera from vertebrate eyes were fixed using 2.5% glutaraldehyde for 1 h at room temperature. Fixed tissue samples were processed for histology and stained using the Warthin–Starry protocol, which tests for the presence of melanin [13].

(d) Scanning electron microscopy

Small samples (approx. 1–2 mm^2) of eye tissue were dried using hexamethyldisilazane or liquid nitrogen. Dried tissue samples and uncoverslipped thin sections were mounted on aluminium stubs, sputter-coated with gold/palladium and imaged at an accelerating voltage of 5–15 keV using an FEI Quanta 650 SEM and a Zeiss Gemini Supra 40 SEM. Energy dispersive X-ray spectroscopy (EDS) analyses were conducted using a Hitachi S-3500N VP-SEM equipped with an EDAX Genesis energy dispersive spectrometer at an accelerating voltage of 15 kV with acquisition times of 120 s for EDS maps (electronic supplementary material, figure S1).

(e) Analysis of melanosome geometry and size

Geometry data were measured for at least 20 melanosomes (and, where applicable, melanosome-like microbodies) for each tissue in each specimen. Differences in geometry were tested using ANOVA or (where data are heteroscedastic) Welch's *F*-test coupled with pairwise post hoc analysis in PAST (Tukey for ANOVA and Dunn for Welch's *F*-test analyses, respectively) [14]. Melanosome geometry data for *S. officianalis* are homoscedastic but non-normal and were thus analysed post-log-transformation.

(f) Synchrotron rapid-scanning X-ray fluorescence

Measurements were performed at beamlines 2-3 and 10-2 at the Stanford Synchrotron Radiation Lightsource (SSRL). The incident X-ray energy was set to 11 keV using a Si (111) double crystal monochromator with the storage ring containing 500 mA in top-off mode at 3.0 GeV. At beamline 2-3, a microfocused beam of 2 × 2 µm was provided by an Rh-coated Kirkpatrick–Baez mirror pair, whereas beamline 10-2 used tungsten apertures to achieve selectable beam sizes between 25 and 200 µm. The incident X-ray intensity at each beamline was measured with a nitrogen-filled ion chamber. Samples were mounted at 45° to the incident X-ray beam and were spatially rastered for 20–50 ms $pixel^{-1}$ dwell time. The following were mapped at beamline 2-3: uncoverslipped and unstained thin sections of eyes from one individual of *Dicentrachus* and *Octopus* and from two individuals of *Loligo* and *Petromyzon*; the eyespots of one specimen of *Tullimonstrum* (CKGM F 6426), *Knightia* sp. and the Teterodontiformes indet. The following were mapped at beamline 10-2: the second specimen of *Tullimonstrum* (FMNH PE 22061), *Mayomyzon*, *Gilpichthys*, *Pohlsepia* and samples of soft tissues from *Keuppia* sp. The two different beamlines were used to accommodate samples/specimens of different sizes (specimens too large for the sample stage at beamline 2-3 were accommodated at 10-2). The fossil data from each beamline were calibrated against the same set of standards and thus, variations in the data are real and do not reflect variations in analytical parameters. The entire fluorescence spectrum was collected at each data point and the intensity of fluorescence lines for selected elements (P, S, Cl, K, Ca, Ti, Mn, Fe, Ni, Cu and Zn) monitored using a silicon drift Vortex detector (Hitachi, USA) coupled to an Xpsress3 pulse processing system (Quantum Detectors) for energy discrimination. Fluorescence intensities were corrected for detector deadtime and normalized against incoming flux (I0STRM). The concentrations of each element in µg cm^{-2} were calibrated using NIST traceable thin film elemental standards. Data processing was performed using the MicroAnalysis Toolkit software [15]. The mean and standard deviation values were calculated for the concentrations of each element in selected regions of interest. Differences in elemental concentrations between regions of interest were assessed using linear discriminant analysis (LDA) in PAST [14]. Data were grouped using a single classification level corresponding to the tissue of origin, e.g. *Octopus* retinal pigmented layer (RPL), *Petromyzon* iris, *Petromyzon* sclera, FMNH PE 22061 eyespot, etc. Principal component analysis of the data produces a distribution of the data that is near-identical to LDA (electronic supplementary material, figure S4*a*,*b*).

(g) X-ray absorption near edge structure spectroscopy

XANES spectra were collected at beamline 2-3 at the SSRL from points of interest identified in the XRF maps. This was achieved by driving the incident beam energy through the Cu K edge in a stepwise fashion and recording the emitted intensity of the Kα line as a function of incident energy [16]. Calibration of the monochromator energy was achieved using a Cu foil. XANES spectra were obtained from the RPL and sclera of *Loligo*, the choroid of *Petromyzon* and from eyespots in the specimen of Tetradontiformes indet., *Knightia* and *Tullimonstrum* (CKGM F 6426). Spectra were processed using the software package Athena [17].

3. Results

(a) Melanin and melanosomes in extant cephalopod and vertebrate eyes

Unexpectedly, several distinct tissue layers in the eyes of all cephalopods studied show black, melanin-specific [13] staining (figure 1). These data are supported by AHPO analyses, which confirm that the stained tissues of *Loligo*, *Octopus* and *Sepia* are rich in eumelanin and, to a lesser extent, phaeomelanin (electronic supplementary material, table S2). SEM analysis of the melanin-rich tissues confirms the presence of spheroid/oblong microbodies (see also [18]; figure 1). It is highly unlikely that the microbodies represent decay bacteria as the former occur within the intact eyes of freshly killed specimens with no evidence of tissue damage, show consistent size-specific layering among specimens of the same taxon and are stable under the electron beam. Further, the microbodies are unlikely to represent ommochrome granules as the former occur in tissue layers that stain positively for melanin in histological section and contain diagnostic markers for eumelanin in AHPO analyses. No other microbodies are present that could generate these results. The microbodies in the tissue layers staining black in histological sections of the cephalopod eyes are thus most plausibly interpreted as melanosomes.

In extant cephalopods, melanosomes occur in the iris and in additional tissue layers located at the back of the eye (defined here as the RPL) and behind the iris (defined here as the subciliary layer (SCL); figure 1*a*,*c*). All cephalopods studied possess an SCL but histological-quality samples of this tissue could be obtained only for *Octopus*. Melanosomes differ significantly in geometry between the iris and RPL in both *Loligo* ($F_{1,90} = 7.275$, $p = 8.35^{-3}$) and *Sepia* ($F_{1,48} = 10.94$, $p = 1.79^{-3}$) (figure 2*a*,*c*). Differences in the geometry of eye melanosomes of *Octopus* and *Petromyzon* are statistically significant for some, but not all, melanosome populations (figure 2*b*,*d*; electronic supplementary material, table S4). In addition to melanosomes, the cephalopod retina contains abundant subangular, irregularly shaped granules (figure 1*c*). This geometry is inconsistent with that of known melanosomes in vertebrates and cephalopods; the granules may thus represent ommatins or other photosensitive pigments, but their identity has yet to be demonstrated chemically. Various tissues in the eye of the lamprey and bass stain for eu- and phaeomelanin (figure 1*b*,*c*); AHPO analysis confirms the presence of melanin in these tissues and demonstrates marked variation in eumelanin concentrations between the eyes of the two vertebrates (electronic supplementary material, table S2).

In summary, our data reveal that melanosomes in different tissues of the eye have significantly different geometries in both extant cephalopods and vertebrates (electronic supplementary material, tables S3 and S4; figure 2).

(b) Chemistry of eye melanosomes

We used SRS-XRF and XANES to test whether trace metal chemistry can distinguish vertebrate from cephalopod eye melanosomes. In the eyes of the extant squid and octopus, only Cu shows striking spatial partitioning (figure 3*a*,*b*): it is enriched in the sclera but not in the melanin-rich RPL (or other tissues). Zn shows subtle partitioning in both cephalopod taxa analysed: it is slightly enriched in the RPL of the octopus and, to a lesser extent, the sclera of the squid. In the vertebrates, however, melanosome-bearing tissues show striking partitioning of Zn (and, in the lamprey, Fe and Cu) (figure 3*c*,*d*). In the lamprey, Fe is enriched in the iris; Zn is enriched in the iris and, especially, the choroid and RPE, and Cu is enriched in all melanosome-bearing tissues. In the bass, Zn is enriched in all melanosome-bearing tissues. In XRF maps of eyes of extant vertebrates, the choroid and RPE cannot be discriminated using trace element chemistry or ultrastructure, necessitating their treatment as a single tissue. We do not consider this to affect our main results as our data from cephalopods and other vertebrate eye tissues show that intra-specific chemical variation is minor relative to interspecific variation (figure 4*a*,*b*). Melanosome-rich tissues in the eyes of extant vertebrates, but not cephalopods, are thus enriched in Zn (and sometimes Fe and Cu) relative to other ocular tissues.

To test whether this signal persists in fossils, we analysed eyespots in two fossil cephalopods and four fossil vertebrates. Except for the Mazon Creek cephalopod *Pohlsepia*, eyespots in all specimens contain melanosome-like microbodies (electronic supplementary material, figure S3). SRS-XRF maps show that eyespots in the fossil vertebrates *Knightia* and Tetradontiformes indet. (figure 3*e*–*f*) are enriched in Ti and Cu relative to the

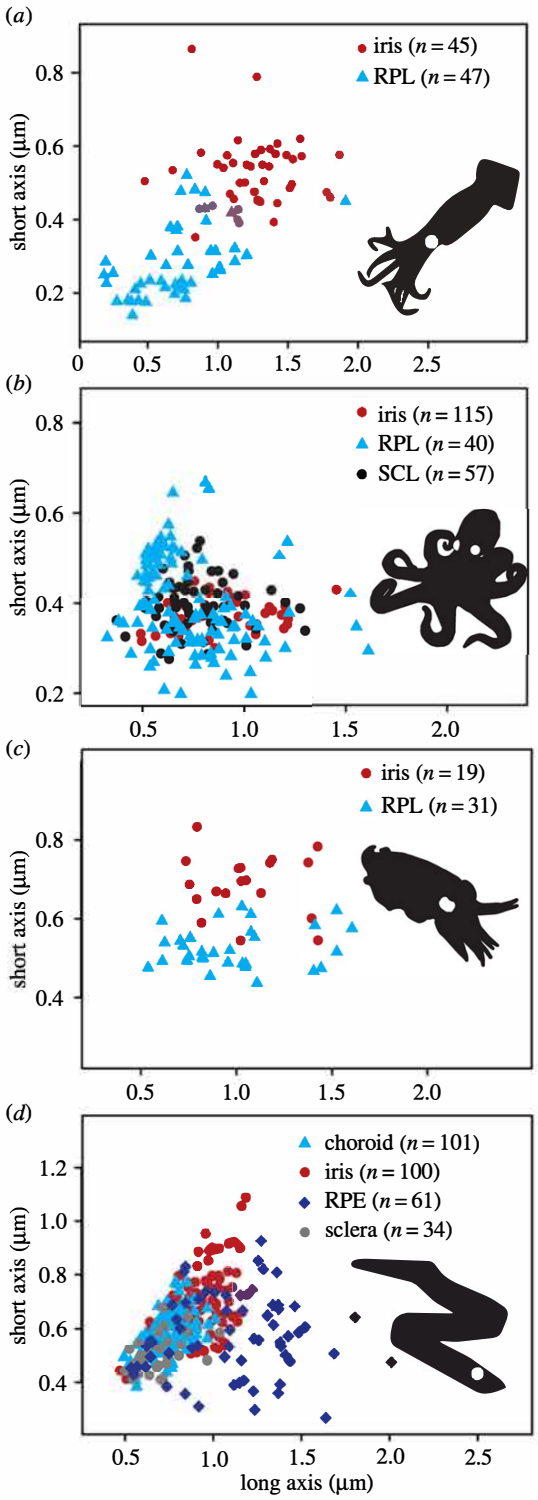

Figure 2. Geometry of eye melanosomes. (*a*) *Loligo*, (*b*) *Octopus*, (*c*) *Sepia* and (*d*) *Petromyzon*.

sedimentary matrix, with minor enrichment of Zn in the latter. By contrast, the eyespot of *Keuppia* is relatively enriched in Ti, Fe and Zn only (figure 3*g*). The eyespot of *Tullimonstrum* is enriched in Ti, Fe, Cu and Zn relative to the surrounding soft tissues (figure 3*h*). These chemical data are not fully consistent with the signal in the studied fossil cephalopods or fossil vertebrates.

We used LDA to explore variation in concentrations of the key elements Ti, Fe, Cu and Zn in our dataset. Eye tissues in

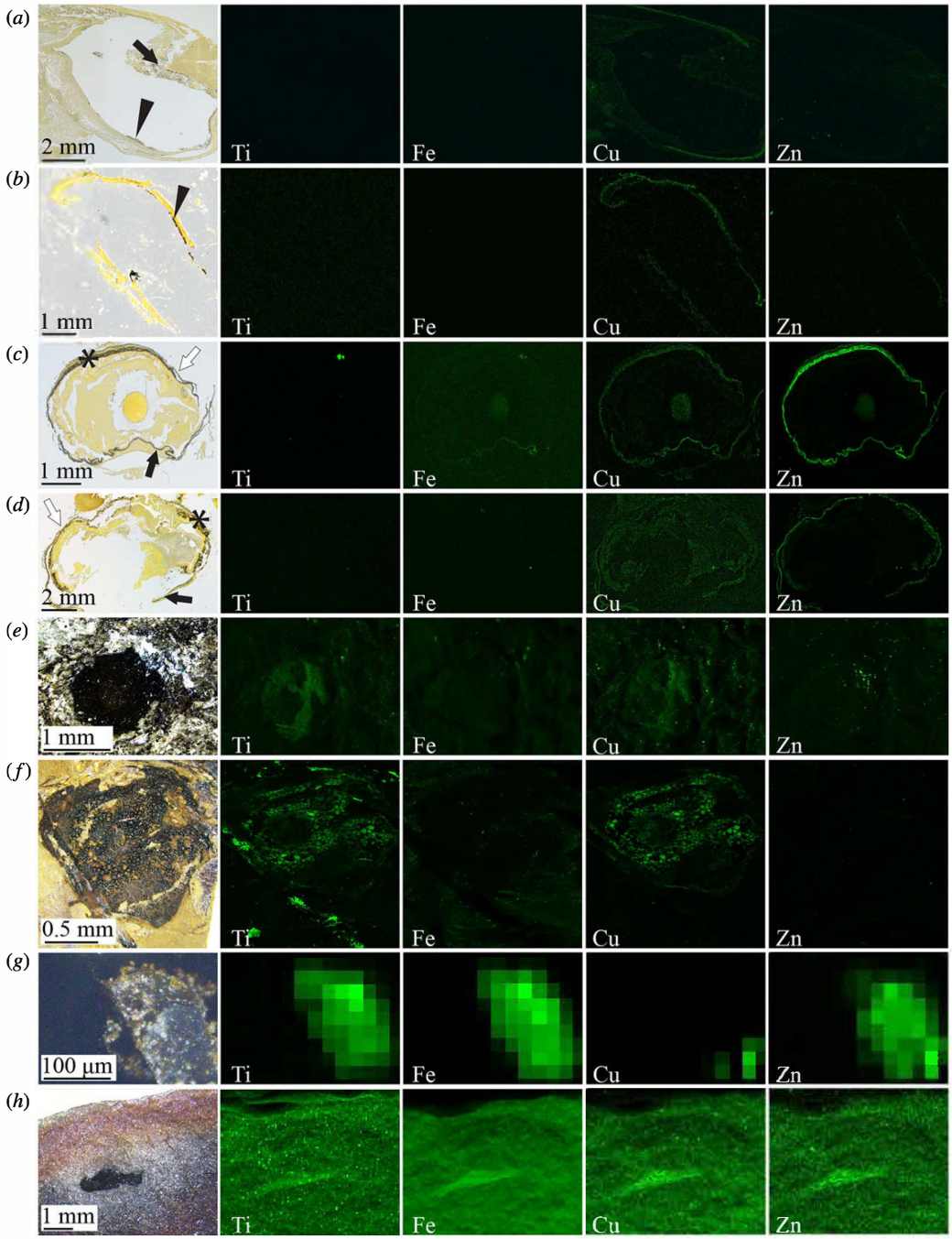

Figure 3. SRS-XRF analysis of histological sections of *Loligo* (*a*), *Octopus* (*b*), *Petromyzon* (*c*) and *Dicentrachus* (*d*), and of fossil vertebrates (Teleostei) Tetradontiformes indet. (*e*) and *Knightia* (*f*), fossil cephalopod *Keuppia* (*g*) and *Tullimonstrum* (CKGM F 6426) (*h*). Histological sections are stained with Warthin–Starry; melanin appears black. SRS-XRF maps in (*a–h*) are of regions shown in histological sections and photographs. See the electronic supplementary material, figure S2 for locations of regions in photographs of histological sections and for locations of regions in photographs of fossils shown. Black arrows, iris; arrowheads, RPL; asterisk, RPE; white arrows, sclera. Maximum concentration values for each SRS-XRF map are provided in the electronic supplementary material, table S5. (Online version in colour.)

extant vertebrates and cephalopods plot in separate regions of chemospace and separately to their fossil counterparts (figure 4*a*,*b*). Critically, the trace element chemistry of eyespots in unequivocal vertebrates from the Mazon Creek is distinct from both specimens of *Tullimonstrum*, which plot close together. The separation of unequivocal Mazon Creek vertebrates from Tullimonstrum along the LD2 axis reflects the enrichment of the former in Zn and, to a lesser extent, Cu and Fe: intriguingly, this mirrors the variation in chemistry between extant vertebrates and cephalopods. The eyespots of *Tullimonstrum* are, however, chemically distinct from those of *Pohlsepia*, an unequivocal cephalopod from the Mazon Creek.

We explored variation in the oxidation state of Cu, a metal commonly associated with melanin [11], in selected fossil and modern taxa using XANES. XANES spectra at the Cu K edge taken from the choroid of the lamprey and from two fossil vertebrate eye spots all show absorption peaks centred at

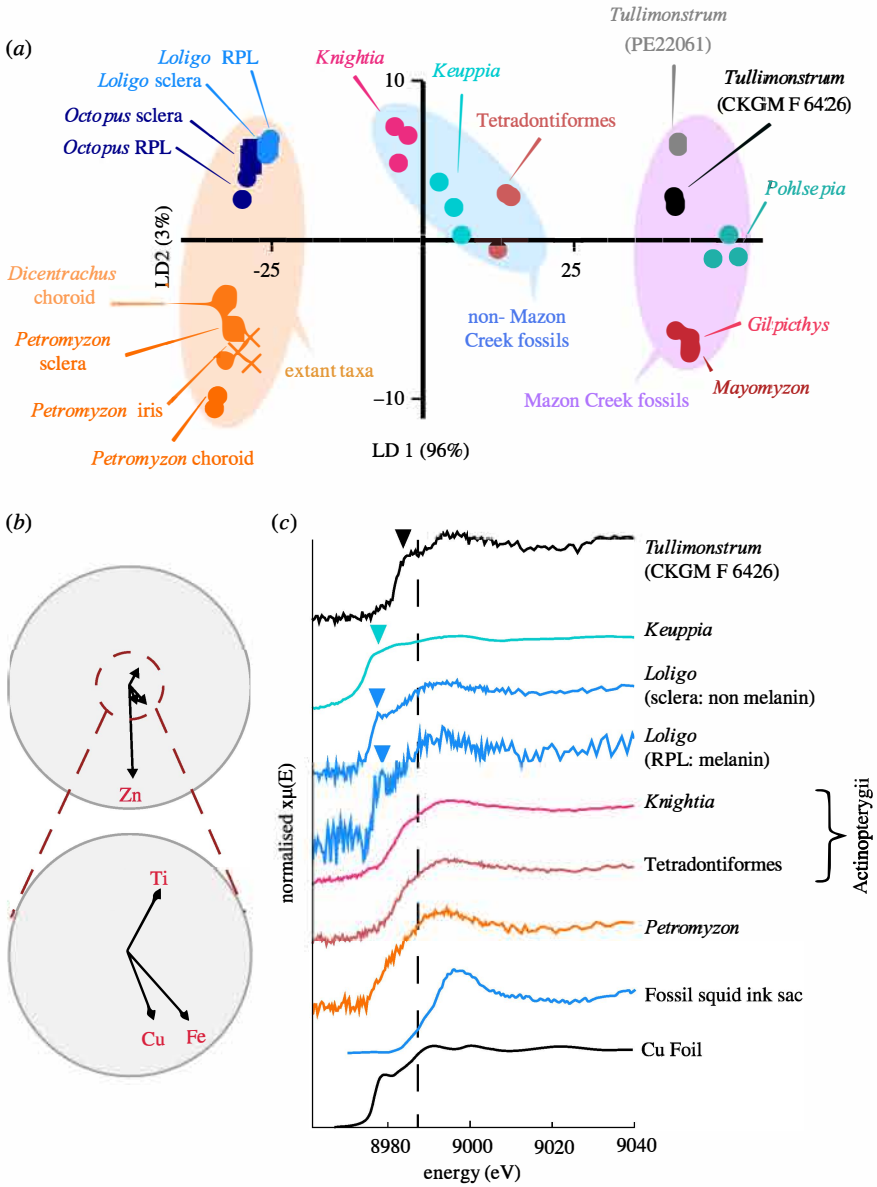

Figure 4. Trace element chemistry of extant and fossil cephalopods and vertebrates and *Tullimonstrum*. (*a*) LDA based on measured concentrations of Ti, Fe, Cu and Zn. (*b*) Biplot of key elements contributing to variation in (*a*). (*c*) XANES spectra of selected specimens and standards at the Cu K edge (dashed line at 8987 eV). The greater variation in chemistry between *Tullimonstrum* and other Mazon Creek fossils present in (*a*) relative to the variation between other fossil biotas is present even when Fe is removed from the dataset (electronic supplementary material, figure S4c,d). Arrowheads in (*c*) indicate the position of pre-edge features in these spectra. Data for fossil squid ink sac are from [16].

8994 ± 1 eV, indicating strong contributions from Cu(II) [19] (figure 4*c*). Spectra from the squid RPL (melanized) and sclera (non-melanized) broadly resemble those of the vertebrates, but show pre-edge features at 8978.59 eV and 8977.58 eV, respectively, the positions of which reveal the presence of Cu(I) [19]. A pre-edge feature spanning 8976.73–8984.27 eV appears in the spectrum from *Keuppia*, also reflecting a Cu(I) contribution. The presence of Cu(I) in XANES spectra of extant and fossil cephalopod eyespots could reflect reduction of Cu(II) during analysis. The vertebrate samples, however, show no contribution from Cu(I) despite being analysed under identical experimental conditions (spectra for some vertebrate samples (e.g. *Knightia*) show very weak pre-edge features, but these are less readily interpreted as unequivocal evidence for Cu(I)). Alternatively, Cu(I) contributions in cephalopod eye tissues could derive from deoxygenated haemocyanin, the cephalopod respiratory molecule [20]. The XANES spectrum from *Tullimonstrum* demonstrates a dominant peak at 8994.38 eV and a prominent pre-edge feature at 8987.8–8990.2 eV. These features are consistent with contributions from multiple Cu oxidation states, including a distinct Cu(I) contribution [19], as with the extant and fossil cephalopods.

4. Discussion

Our study reveals that the eyes of extant cephalopods possess melanosomes with tissue-specific geometries. The collapse of the cephalopod eye during decay could potentially generate size-specific layers of melanosomes superficially similar to those in the vertebrate RPE (figure 1*a*,*b*). The presence of melanosomes with tissue-specific sizes and/or geometries in the

eyes of extant cephalopods (figure 2*a*,*c*) therefore indicates that successive layers of melanosomes of different sizes and/or geometries in fossils cannot be automatically interpreted as evidence for the vertebrate RPE. The extent to which other fossil invertebrate groups preserve eye melanosomes is unknown (but see Lindgren *et al*. [21] for chemical evidence for melanin in the eyes of fossil insects).

Melanin in the eyes of extant vertebrates can bind various elements, the relative abundance of which can vary with biological and environmental factors [22]. In vertebrates, melanin can sequester metal ions, potentially preventing oxidative tissue damage [11]. Compared to vertebrates, cephalopod eyes show low concentrations of metals in melanized tissues (figure 3*a*,*b*). This probably reflects the relatively low abundance of melanin (electronic supplementary material, table S2) and suggests that non-melanin pathways are responsible for preventing tissue damage from metal ion exposure in cephalopods, i.e. the function of melanin in cephalopod eyes differs to that in vertebrates. The variation in melanin content in extant vertebrate eyes (electronic supplementary material, table S2) could potentially reflect variations in ecology and/or light habitat.

Our chemical data on extant vertebrates and cephalopods show that inter-clade variation is markedly greater than that within either group (figure 3*a–d*). The melanized tissues in the eyes of extant vertebrates are enriched in Zn (figure 4*a*,*b*) and show a strong Cu(II) signal in XANES spectra (figure 4*c*); in contrast, melanized tissues in extant cephalopods are low in Zn and show a mixed contribution from Cu(I) and Cu(II). Similarly, eye melanosomes in *Tullimonstrum* are low in Zn relative to those in Mazon Creek vertebrates and XANES spectra indicate the presence of Cu(I). The eye spots in *Pohlsepia*, however, do not plot with *Tullimonstrum* or with the Mazon Creek vertebrates in LDA chemospace. The chemistry of the unequivocal vertebrates and cephalopods in the Mazon Creek thus does not fit the general pattern of element enrichment in modern cephalopods and vertebrates. Collectively, the data on melanosome morphology and chemistry are not fully consistent with a vertebrate affinity for *Tullimonstrum*. An invertebrate affinity [23–25] cannot be excluded, but a cephalopod affinity is implausible, given the absence of other diagnostic morphological characters [26].

The chemical structure of melanin is known to be altered by changes in pH [11] and exposure to elevated metal concentrations [27], pressures and temperatures [28], all of which are commonly experienced during diagenesis. It is therefore likely that melanosomes in different fossil taxa from the same or different biotas may follow different diagenetic pathways, thus resulting in disparate trace element chemistries (as is apparent in studies of the organic geochemistry of fossil melanins [28]). The chemical variation among fossils observed herein (figure 3*e–h*) presumably reflects variation in host lithology and/or diagenetic history. For instance, the absence of preserved melanosomes in *Pohlsepia* suggests that this specimen experienced more extensive alteration during diagenesis than the other fossil specimens analysed. Further, variation in trace element chemistry among Mazon Creek fossils is greater than for fossils from all other biotas. This suggests that the chemical diagenesis of melanosomes in Mazon Creek fossils is more variable than that for other biotas, precluding conclusive interpretation of original trace element chemistry. Nevertheless, the eyes of *Knightia* and the specimen of Tetradontiformes indet. have similar trace metal signatures despite being from different biotas and thus presumably having different diagenetic histories. Future studies targeting the response of melanosome trace element chemistry to various diagenetic factors, e.g. pH, lithology, pressure and temperature, will be critical to discrimination of original chemistry from chemical products of diagenesis.

Data accessibility. We provide all data in the main text, electronic supplementary material or via the Dryad Digital Repository: https://doi.org/10.5061/dryad.c5c7601 [29].

Authors' contributions. C.S.R. and T.I.A. performed histology; C.S.R., T.I.A. and M.E.M. performed SEM; C.S.R., M.E.M. and S.M.W. performed synchrotron rapid scanning-X-ray fluorescence and X-ray absorption spectroscopy (XAS); S.I. and K.W. performed AHPO analyses; C.S.R. and M.E.M. wrote the manuscript with input from all other authors.

Competing interests. The authors declare no competing interests.

Funding. Supported by European Research Starting Grant (grant no. ERC-2014-StG-637691-ANICOLEVO) awarded to M.E.M. The use of the Stanford Synchrotron Radiation Lightsource, SLAC National Accelerator Laboratory, is supported by the US Department of Energy, Office of Science, Office of Basic Energy Sciences under contract no. DE-AC02-76SF00515.

Acknowledgements. We thank A. Aase, S. Gabbott, Z. Hughes, R. Gaines, B. Lindow, P. Mayer, D. Mikulic, W. Simpson and A. Stroup for access to specimens; N. Edwards for XAS support; V. Rossi and R. Wogelius for discussion.

References

1. Oakley TH, Speiser DI. 2015 How complexity originates: the evolution of animal eyes. *Annu. Rev. Ecol. Evol. Syst.* **46**, 237–260. (doi:10.1146/annurev-ecolsys-110512-135907)
2. Clements T, Dolocan A, Martin P, Purnell MA, Vinther J, Gabbott SE. 2016 The eyes of *Tullimonstrum gregarium* (Mazon Creek, Carboniferous) reveal a vertebrate affinity. *Nature* **532**, 500–503. (doi:10.1038/nature17647)
3. Liu Y, Hong L, Wakamatsu K, Ito S, Adhyaru BB, Cheng C-Y, Bowers CR, Simon JD. 2005 Comparisons of the structural and chemical properties of melanosomes isolated from retinal pigment epithelium, iris and choroid of newborn and mature bovine eyes. *Photochem. Photobiol.* **81**, 510–516. (doi:10.1562/2004-10-19-RA-345.1)
4. Durairaj C, Chastain JE, Kompella UB. 2012 Intraocular distribution of melanin in human, monkey, rabbit, minipig and dog eyes. *Exp. Eye Res.* **98**, 23–27. (doi:10.1016/j.exer.2012.03.004)
5. Zhang QX, Lu RW, Messinger JD, Curcio CA, Guarcello V, Yao XC. 2013 *In vivo* optical coherence tomography of light-driven melanosome translocation in retinal pigment epithelium. *Sci. Rep.* **3**, 2644. (doi:10.1038/srep02644)
6. Fernald RD. 2000 Evolution of eyes. *Curr. Opin Neurobiol.* **10**, 454–450. (doi:10.1016/S0959-4388(00)00114-8)
7. Palumbo A. 2003 Melanogenesis in the ink gland of *Sepia officinalis*. *Pigment Cell Res.* **16**, 517–522. (doi:10.1034/j.1600-0749.2003.00080.x)
8. Schraermeyer U. 1994 Fine structure of melanogenesis in the ink sac of *Sepia officianalis*. *Pigment Cell Melanoma Res*. **7**, 52–60. (doi:10.1111/j.1600-0749.1994.tb00018.x)
9. Ito S, Miyake S, Maruyama S, Suzuki I, Commo S, Nakanishi Y, Wakamatsu K. 2018 Acid hydrolysis

reveals a low but constant level of pheomelanin in human to black to brown hair. *Pigment Cell Melanoma Res.* **31**, 393–403. (doi:10.1111/pcmr.12673)
10. Wakamatsu K, Ito S, Rees JL. 2002 The usefulness of 4-amino-3-hydroxyphenylalanine as a specific marker for pheomelanin. *Pigment Cell Res.* **15**, 225–232. (doi:10.1034/j.1600-0749.2002.02009.x)
11. Hong L, Simon JD. 2007 Current understanding of the binding site, capacity, affinity, and biological significance of metals in melanin. *J. Phys. Chem. B* **111**, 7938–7947. (doi:10.1021/jp071439h)
12. Rossi V, McNamara ME, Webb S, Ito S, Wakamatsu K. 2019 Tissue-specific geometry and chemistry of modern and fossilized melanosomes reveal internal anatomy of extinct vertebrates. *Proc. Natl Acad. Sci. USA* **116**, 17 880–17 889. (doi:10.1073/pnas.1820285116)
13. Joly-Tonetti N, Wibawa JID, Bell M, Tobin D. 2016 Melanin fate in the human epidermis: a reassessment of how best to detect and analyse histologically. *Exp. Dermatol.* **25**, 501–504. (doi:10.1111/exd.13016)
14. Hammer Ø, Harper DAT, Ryan PD. 2001 PAST: paleontological statistics software package for education and data analysis. *Palaeontol. Electron.* **4**, 9.
15. Webb SM. 2011 The microanalysis toolkit: X-ray fluorescence image processing software. *AIP Conf. Proc.* **1365**, 196–199. (doi:10.1063/1.3625338)
16. Wogelius, RA *et al*. 2011 Trace metals as biomarkers for eumelanin pigment in the fossil record. *Science* **333**, 1622–1626. (doi:10.1126/science.1205748)
17. Ravel B, Newville M. 2005 Athena, Artemis, Hephaestus: data analysis for X-ray absorption spectroscopy using IFEFFIT. *J. Synchrotron Radiat.* **12**, 537–541. (doi:10.1107/S0909049505012719)
18. Schraermeyer U, Stieve H, Rack M. 1995 Immunoelectron-microscopic study of G-protein distribution on photoreceptor cells of the cephalopod *Sepia officinalis*. *Tissue Cell* **27**, 317–322. (doi:10.1016/S0040-8166(95)80052-2)
19. Kau LS, Spira-Solomon DJ, Penner-Hahn JE, Hodgson KO, Solomon EI. 1987 X-ray absorption edge determination of the oxidation state and coordination number of copper: application to the type 3 site in *Rhus vernicifera* Laccase and its reaction with oxygen. *J. Am. Chem. Soc.* **21**, 6433–6442.
20. Coates CJ, Nairn J. 2014 Diverse immune functions of hemocyanins. *Dev. Comp. Immunol.* **45**, 43–55. (doi:10.1016/j.dci.2014.01.021)
21. Lindgren J *et al*. 2019 Fossil insect eyes shed light on trilobite optics and the arthropod pigment screen. *Nature* **573**, 122–125.
22. Hong L, Simon JD. 2005 Physical and chemical characterization of iris and choroid melanosomes isolated from newborn and mature cows. *Photochem. Photobiol.* **81**, 517–523. (doi:10.1562/2005-03-02-RA-453.1)
23. Sallan L, Giles S, Sansom RS, Clarke JT, Johanson Z, Sansom IJ, Janvier P. 2017 The 'Tully Monster' is not a vertebrate: characters, convergence and taphonomy in Palaeozoic problematic animals. *Palaeontology* **60**, 149–157. (doi:10.1111/pala.12282)
24. Foster M. 1979 A reappraisal of *Tullimonstrum gregarium*. In *Mazon creek fossils* (ed. MH Nitecki), pp. 269–301. New York, NY: Academic Press.
25. Beall B. 1991 The Tully Monster and a new approach to analysing problematica. In *The early evolution of Metazoa and the significance of problematic taxa: international symposium* (eds S Conway-Morris, AM Simonetta), pp. 271–286. Cambridge, UK: Cambridge University Press.
26. Smith MR, Caron J-B. 2010 Primitive soft-bodied cephalopods from the Cambrian. *Nature* **465**, 469–472. (doi:10.1038/nature09068)
27. Chen S, Xue C, Wang J, Feng H, Wang Y, Ma Q, Wang D. 2009 Adsorption of Pb(II) and Cd(II) by squid *Ommastrephes bartrami* melanin. *Bioinorg. Chem. Appl.* **2009**, 901563. (doi:10.1155/2009/901563)
28. Colleary C *et al*. 2015 Chemical, experimental and morphological evidence for diagenetically altered melanin in exceptionally preserved fossils. *Proc. Natl Acad. Sci. USA* **112**, 12 592–12 597. (doi:10.1073/pnas.1509831112)
29. Rogers CS, Astrop TI, Webb SM, Ito S, Wakamatsu K, McNamara ME. 2019 Data from: Synchrotron X-ray absorption spectroscopy of melanosomes in vertebrates and cephalopods: implications for the affinity of *Tullimonstrum*. Dryad Digital Repository. (https://doi.org/10.5061/dryad.c5c7601)